International Journal of Chemical and Biochemical Sciences
(ISSN 2226-9614)

Journal Home page: www.iscientific.org/Journal.html

Therapeutic efficacy of capecitabine in combination with salinomycin and / or graphene oxide nanoparticle on experimentally induced hamster buccal pouch carcinoma

Ahmed Alnos Aly[1*], Khaled Mohamed Afify[2], Mohamed Mahmoud Ahmed[3]

[1]Assistant lecturer, Oral and Dental Pathology department, Faculty of Dental Medicine, Assiut, Al-Azhar University, Egypt

[2]Assistant Professor, Department of Oral and Dental Pathology Faculty of Dental Medicine, Assiut, Al-Azhar University, Egypt

[3]Professor, and head of Oral and Dental Pathology department, Faculty of Dental Medicine, (Boys Cairo), Al-Azhar University, Egypt

Abstract

Current research has been directed to examine the therapeutic effect of capecitabine in combination with Salinomycin and/or graphene oxide (GO) nanoparticles on experimentally induced hamster buccal pouch carcinoma. 70 Syrian male hamsters 5weeks old, weighing80-120g, had been split into 7groups (10 in each). GI: Animals left untreated. GII: Animals had been painted with 0.5percent 7, 12-dimethylbenz (a) anthracene to induce cancer (three times/week/fourteen weeks). GIII: DMBA had been applied as inGII followed by treatment with capecitabine only. GIV: DMBA was applied as in GII followed by treatment with GO. GV: DMBA was applied as in GII followed by treatment with capecitabine and salinomycin. GVI: DMBA was applied as in GII followed by treatment with capecitabine and GO. GVII: DMBA was applied as in GII followed by treatment with capecitabine, salinomycin, and GO. At the end of the experiment, animals had been euthanized, then all right pouches had been excised, & split into 2 specimens. 1 specimen had been prepared to be examined histologically and immunohistochemistry (IHC). Other specimens of fresh tissue had been mechanically digested, suspended, & conjugated with annexin V FITC /propodium iodide (PI). Gross observations and histopathological examination revealed some variability of anticancer effect across the medicated groups (GIII, GIV, GV, GVI, and GVII) contrasted to GII, with the synergistic antitumor effect of GVII compared to other medicated groups. According to IHC staining of ALDH1A1, cancer stem cells (CSCs) increased in GII and reached the highest level in GIII. While the CSCs population decreased in other medicated groups, reached to least population in GVII. According to flowcytometric (FCM) detection of apoptosis using annexin V /PI assay, apoptosis increased in medicated groups compared to GII and reached to highest percentage in GVII. Combining three active cytotoxic agents including capecitabine, Salinomycin, and GO improves anticancer efficacy by inhibiting growth and inducing apoptosis, targeting CSCs by differentiation or eradication, overcoming chemoresistance, and sensitizing tumor cells.

Keywords: Capecitabine, Salinomycin, Graphene oxide, HBP carcinoma, CSCs.

Full length article **Corresponding Author*, e-mail: ahmedalnos16@gmail.com

1. Introduction

Over ninety percent of oral cancer cases worldwide are oral squamous cell carcinoma, which has become more common in the present years [1]. OSCC is classified as one of the most aggressive malignant tumors because of its propensity to spread & increase in recurrence [2]. There are several alternatives for treatment, such as radiation, chemotherapy, surgery, or a combination thereof [3]. While numerous chemotherapy therapies are demonstrated to elicit responses, increasing survival is still an unmet objective [4]. Chemoresistance raises the risk of metastasis & results in poor long-term prognosis, which makes it a significant obstacle to cancer treatment [5].

Tumor-initiating cells, known as cancer stem cells, are tiny subpopulations of cancer cells that have the capacity for both unrestricted self-renewal & tumor development [6]. These cells can self-renew & differentiate thanks to a variety of intracellular signal transduction pathways. They may be involved in a variety of cancers. Additionally, as they are resistant to established treatment approaches that primarily target most tumor cells, they play a significant role in tumor spread & recurrence [7]. Hamster buccal pouch (HBP) has been the most well-characterized animal model for the development of oral cancer, even though various other models have been created. Topical administration of 7,12-dimethylbenz-[a]-anthracene (DMBA) for twelve to fourteen weeks results in the development of human oral malignancies, closely matching frequent occurrences in the HBP model, which was first reported in the literature [8-9]. DMBA has been considered a potent chemical carcinogen as it can induce precancerous lesions and carcinomas within a few weeks of its topical administration [10]. One prodrug of oral fluorouracil is capecitabine (Xeloda). It may be transformed into 5-fluorouracil (5-FU) upon intake in the liver & in tumor cells that have thymidine phosphorylase (TP), which may increase intra-tumoral concentrations of fluorouracil [11]. Capecitabine is a member of the antimetabolite class that exhibits a cytotoxic effect by inhibiting thymidylate synthase (TS) & allowing its metabolites to be incorporated into ribonucleic acid (RNA) & deoxyribonucleic acid (DNA) [12]. It has revealed clinically meaningful antitumor activity in the spectrum of cancer types containing OSCC [13]. Different mechanisms have been identified accounting for cancer cells' resistance to capecitabine, therefore, combination cancer therapies seek to improve therapeutic responses & decrease the likelihood of acquired resistance in individual studied cases [14]. Salinomycin is a polyether ionophore antibiotic used in the poultry industry [15]. Because salinomycin exhibits strong action against a variety of cancer cell types, particularly those that exhibit multi-drug resistance & CSC, it is very intriguing [16]. Salinomycin may specifically destroy CSCs through several processes, such as necrosis, autophagy, & apoptosis [17]. In vivo & in vitro, salinomycin effectively inhibits proliferation, induces cell death, & suppresses metastasis in human malignancies of various origins without having the same detrimental effects on the body as traditional chemotherapy medicines [18]. Graphene oxidation yields graphene oxide nanoparticles, which are rich in carboxylic & hydroxyl functional groups [19]. GO has demonstrated a lot of promise for biological & therapeutic uses [20]. Some tumor cells have been reported to be inhibited by GO. GO may target CSCs specifically. It also induces CSC differentiation & inhibits tumor-sphere formation in a variety of cell lines, like breast, ovarian, prostate, lung, pancreatic, & glioblastoma. It does this by blocking several important signaling pathways, like Wnt, Notch, & signal transducer & activator of transcription signaling. This phenomenon was given the term "differentiation-based nano-therapy" by the researchers [21]. Therefore, the main target of the present study is to investigate the efficacy of capecitabine in combination with salinomycin and/or GO nanoparticles on experimentally induced HBP carcinoma.

2. Material & methods

2.1. Experimental animals

70 male Syrian hamsters, aged 5weeks & weighing between 80 & 120 grams, had been acquired from Cairo University's animal house in Cairo, Egypt. Experimental animals had been kept in standard cages with sawdust bedding under controlled temperature (22 ± 2°C), humidity (thirty to forty percent), & light (12hours of light & 12 hours of darkness). Every experimental animal was fed a regular meal & had access to water. Animal Research Unit of Faculty of Pharmacy, Cairo, Boys, Al-Azhar University is where the experiment had been carried out. experiment was conducted in compliance with worldwide criteria for biomedical research with animals as well as guidelines of the Medical Research Institute [22]. The procedures had been accepted by ethical & research committee protocol of Faculties of Dental Medicine and Pharmacy, Cairo, Boys, Al-Azhar University.

2.2. Materials

DMBA 0.5% (Sigma-Aldrich Company, USA), dissolved in paraffin oil. Capecitabine had been purchased from the pharmacy as a Xeloda tablet 500mg (Genentech USA Inc. a member of Roche group). Salinomycin (Sigma-Aldrich Company, USA). GO had been purchased as a nano colloid (Sigma-Aldrich Company, USA).

2.3. Experimental design

After 1week of adaptation animals had been separated into7 groups of 10 hamsters in each group: GI (normal group) animals, had been fed & watered only & served as negative controls. GII (DMBA) in which the right HBP had been painted with0.5 percent DMBA in liquid paraffin using number four camel's hairbrush three times in 1week, for 14 weeks, and served as positive controls [23]. GIII (capecitabine) in which DMBA was applied as in GII to induce OSCC followed by administration of capecitabine orally by plastic oral gavage, 600mg/kg/day, daily for a week followed by a week of rest, then a week of treatment [24]. GIV (GO) in which animals were painted with DMBA as in GII then GO was injected directly into the tumor by insulin syringe, 2 mg/kg/ day [25]. GV (capecitabine + salinomycin) in which animals were painted with DMBA as in GII then capecitabine was administered as in GIII in addition to salinomycin which was intraperitoneally injected by insulin syringe, 10 mg/kg/ day [26]. GVI (capecitabine + GO) in which animals were painted with DMBA as in GII then capecitabine was administered as in GIII in addition to GO which was administrated as in GIV. GVII (capecitabine + salinomycin + GO) in which animals were painted with DMBA as in GII then capecitabine was administrated as in GIII, salinomycin was administrated as in GV, in addition to GO which was administrated as in GIV.

2.4. Gross examination, sample collection, and preparation

After end of experiment, animals had been euthanized, & right HBPs were excised & grossly examined. Each HBP had been split into 2 specimens. 1 specimen had been fixed in ten percent neutral buffered formalin for 48 hours to be prepared for histological and IHC examination.

Another part of a specimen of fresh tissue had been mechanically digested, suspended & conjugated with annexin V/ PI using an annexin staining kit as per manufacturer's instructions.

2.5. Histological examination

Tissues that underwent a sequence of alcohol solutions for dissection & dehydration, xylene cleaning, paraffin wax infiltration, & paraffin block embedding. Sections of tissue had been cut to a thickness of 5µ, &histological results had been regularly recorded & examined using hematoxylin & eosin (H & E) staining.

2.6. Measurement of depth of invasion

Using H & E slide, the DOI of each surgical specimen had been ascertained. depth of tumor infiltration was determined by calculating DOI starting from the basal layer of surface epithelium. It has been further classified as less invasive at ≤ five mm, moderately invasive at6-10mm, & extremely invasive at ≥10mm by the American Joint Committee on Cancer (Figure 1) [27]. Leica QWIN V3 image analyzer computer system (Switzerland) running Leica QWIN V3 software had been used to calculate DOI. This had been carried out at Al-Azhar University in Egypt's Department of Oral & Dental Pathology, Faculty of Dental Medicine (Boys-Cairo).

2.7. Immunohistochemical examination

Paraffin blocks had been cut into four µm thick sections & mounted on positively charged glass slides. After deparaffinizing & rehydrating slides, 0.01M citrate buffer (pH 6.0) was used to extract the antigen. Slides were treated for fifteen minutes in three percent aqueous hydrogen peroxide to quench endogenous peroxidase activity, then for 20 minutes. At room temperature in Protein Block Serum-Free (Dako, CA, USA) to reduce nonspecific binding of the following reagents [28]. Tissue sections received 1 or 2 drops of primary antibodies (polyclonal goat anti-mouse aldehyde dehydrogenase1A1 (ALDH1A1) antibody (Catalog# AF5869) R & D systems, Bio-techne) in dilution of 1:15 & incubated in humid chamber at 4°C overnight. After that, the slides had been cleaned with distilled water & then PBS for 5minutes. After adding the biotinylated anti-goat secondary antibody, the mixture had been incubated for thirty minutes at room temperature. After applying 1 or 2 drops of peroxidase-labeled streptavidin for 30 minutes at room temperature, samples were cleaned in PBS. Finally, the slides had been stained with DAB and hematoxylin, & covered with plastic covers to be checked. Primary antibody was left out of the preparation of negative controls. Human prostate tissue was employed as ALDH1A1 positive control (Figure 2). To determine the location of immunostaining within tissues & frequency of positive instances, immune stained slices were inspected under a light microscope. A computerized image analysis method was also utilized to verify area percentage of immunostaining cells positive for ALDH1A1. This had been carried out at Al-Azhar University in Egypt's Department of Oral & Dental Pathology, Faculty of Dental Medicine (Boys-Cairo). degree of positive staining for antibodies had been assessed by well-established semi-quantitative scoring on scale range from negative (0-5%), mild (6-25%), moderate (26-50%) to strong positive staining (More than 50%).

2.8. FCM detection of apoptosis using annexin V/ PI assay

Tissue suspension was prepared from fresh tissue specimens according to Tribukait as stated below [29]. Biopsy specimens were transported to the laboratory in isotone saline. Tumor tissue specimens were disaggregated manually, gently minced, and gently squeezed through a nylon mesh of 100µm pore diameter with isotone Tris EDTA (3.029gm of 0.1M tris hydroxymethyl aminomethane (cat. No. T-1378, sigma chemical company), 1.022gm of 0.07M sodium chloride (ADWIC) & 0.47gm of 0.005M EDTA (cat. No. E-6758, sigma) had been dissolved in 250mL of distilled water & pH had been adjusted at 7.5using (1N HCl). Then, cell suspension had been centrifuged at 1800 rpm for ten min, whereupon supernatant had been aspirated. After centrifugation & aspiration of supernatant, cells had been fixed in ice-cold ninety-six to one hundred percent ethanol in about one ml for each sample.

2.9. Staining method of annexin V kit (cat. No.556547BD pharmingen FITC apoptosis Kit)

1- 100 µl of cells suspensions was added onto 5ml test tube & then resuspended in 100ml of1x binding buffer (1ml of10x buffer +9ml dist. H20). 2- 100 µl of cell suspension were taken in another 5ml test tube then5µl of annexin V (FITC label) & directly 5µl PI (Phycoerythrin label) had been added, & then incubated in dark at room temperature for fifteen minutes. 3- Control was prepared by incubating cells in the absence of an inducing agent. 4- cell was ready for acquisition on FCM. The FCM analysis was performed on the Accruri C6 cytometer (Becton Dickinson (BD), Sunnyvale, CA, USA) in Mansoura Children Hospital, which is equipped with blue & red laser, 2 light scatter detectors & 4fluorescence detectors with optical filters optimized for recognition of numerous popular fluorochromes, containing FITC (blue fluorescence) and PE (red fluorescence) with laser beam 488nm wavelength. average number of calculated nuclei per specimen had been 20.000 & the number of nuclei checked had been120/s. Using Accuri C6 software (Becton Dickinson) for data analysis. 4 quadrants (UL: upper left; UR: upper right; LL: lower left; LR: lower right) had been created for the scatterplots. Living, non-apoptotic cells in LL quadrant are shown to be negative for both annexin V & PI. While UR quadrant displays late apoptosis cells positive for both annexin V & PI UL quadrant displays dead cells, which are positive for PI but negative for annexin V. Living, early apoptotic cells are seen in LR quadrant; they are positive for annexinV but negative for PI.

2.10. Statistical analysis

The mean & standard deviation of the data had been computed after statistical analysis. Version 24 of Statistical Program for Social Science (SPSS) had been used to conduct a one-way analysis of variance (ANOVA). ANOVA had been used in conjunction with a post hoc least significant difference test to distinguish between more than 2 distinct groups when dealing with quantitative data & parametric distribution.

Pertinent probability (p-values) had been utilized to determine significance: $p < 0.05$ indicates significance, $p > 0.05$ indicates non-significant, & $p < 0.001$ indicates high significance.

3. Results

3.1. Gross observations

GI showed no observable abnormalities. The mucosa appeared pink in color with a smooth surface during experiment period Fig. (3A). GII animals revealed a whitish membrane and roughened granular surface on pouch mucosa, with varying degrees of erythema & multiple exophytic nodules of variable size surrounded with area of ulceration & bleeding Fig. (3B). Multiple nodules usually confluent and appearing as large single mass (fungating tumor masses). These large lesions had also spread to contiguous tissue so that the buccal pouch was fixed and could not be everted with the tumor Fig. (3C). GIII Animals showed marked reduction in size & number of exophytic masses as compared to GII with area of bleeding in some animals Fig. (3D). GIV animals showed relative reduction in size & number of exophytic masses as compared to GII, but less than GIII. Fig. (3E). GV animals showed marked reduction in size & number of exophytic masses as compared to GII, GIII, and GIV with the absence of erosive, inflammation, and bleeding surfaces around masses. Animals appeared marked improvement in general health and body weight gain was noticed Fig. (3F). GVI animals showed marked reduction in size & number of exophytic masses as compared to GII, GIII, and GIV Fig. (3G). GVII animals showed rough whitish granular surfaces, mild erythema, and some tiny red exophytic lesions. There had been a significant reduction in the size of exophytic masses rather than other animals in this study with the absence of ulceration and bleeding. All hamsters showed noticeable improvement in general health compared to other groups Fig. (3H).

3.2. Histopathological & IHC results

- GI: lining epithelium of HBP mucosa seemed normal and thin with three to five cells thick keratinized stratified squamous epithelium, according to histological sections stained with H&E. There were no rete processes and epithelium-connective tissue (CT) interface had been comparatively flat. There had been no damage to the basement membrane. subepithelial CT and muscular layer had been seen Fig. (4A). IHC staining using ALDH1A1 exhibited negative cytoplasmic expression (mean = 4.1%) which limited to basal & supra basal epithelial layers Fig. (6A).
- GII: H & E stain revealed that 8 cases exhibited well-differentiated SCC & 2 cases exhibited moderate SCC. In well-differentiated SCC the CT had been invaded deeply by malignant epithelial cells and may reach to muscle layer. Invasive epithelial cells appeared as epithelial nests with keratin pearls. Tumor cells with hyperchromatic, pleomorphic nuclei exposed changed nuclear/cytoplasmic ratio. Multiple dysplastic characteristics and basement membrane destruction Fig. (4B). Moderate SCC was composed of cords or islands of neoplastic atypical epithelial cells, oval-shaped or round which infiltrated tumoral stroma with less keratin formation Fig. (4C). The mean of DOI was 10.4mm. IHC staining using ALDH1A1 exhibited moderate positive cytoplasmic expression (mean = 26.8%) during epithelial layers and throughout cells of tumor nests as brownish cytoplasmic staining and notably absent in the center of keratin pearls. The expression was mainly scattered in separated tumor cells or appeared as a patchy pattern Fig. (6B, C).
- GIII: H & E stain revealed that 6 animals exhibited well-differentiated SCC & 4 animals exhibited severe dysplasia. Well-differentiated squamous cells with invading islands to underlying CT showed invasive SCC which did not invade deeply into underlying CT & nests appeared less in size with the presence of fibrosis surrounding small epithelial tumor nests, which verified regression of tumor Fig. (4D). The meaning of DOI was 3.18mm. IHC staining using ALDH1A1 exhibited moderate positive cytoplasmic expression (mean = 41.1%) during epithelial layers and throughout cells of the tumor nests. The expression was mainly scattered in separated tumor cells or appeared as a patchy or diffuse pattern Fig. (6D).
- GIV: H & Estain revealed that 7 animals exhibited well-differentiated SCC & 3 animals exhibited severe dysplasia. Well-differentiated squamous cells showed invasive SCC which did not invade deeply into the underlying CT Fig. (4E). The mean of DOI was 3.9mm. IHC staining using ALDH1A1 exhibited mild positive cytoplasmic expression (mean = 17.4%) scattered during epithelial layers and throughout cells of the tumor nests. The expression was mainly scattered in separated tumor cells or appeared as a patchy pattern Fig. (6E).
- GV: H & E stain revealed that 3 animals exhibited well differentiated SCC, 6 animals exhibited sever dysplasia and 1 animal exhibited moderate dysplasia. Well-differentiated squamous cells with invading islands to underlying CT showed superficial invasive SCC and often developed large amounts of keratin Fig. (4F). The mean of DOI was 1.46 mm. The IHC staining using ALDH1A1 exhibited mild positive cytoplasmic expression (mean = 14.2%) localized to basal and supra basal layers and scattered around peripheral cells of tumor nests Fig. (6F).
- GVI: H & E stain revealed that 5 animals exhibited well-differentiated SCC, 4 animals exhibited severe dysplasia & 1 animal exhibited moderate dysplasia. Lesions had been well-differentiated and did not invade deeply into underlying CT Fig. (4G). The mean of DOI was 1.93mm. IHC staining using ALDH1A1 exhibited mild positive cytoplasmic expression (mean = 22.4%) localized to the basal & supra basal layers and around peripheral cells of tumor nests Fig. (6G).

- GVII: H & E stain revealed that 2 animals exhibited well-differentiated SCC, 4 animals exhibited severe epithelial dysplasia, 3 animals exhibited moderate dysplasia & animals exhibited mild dysplasia. In 2 hamsters of SCC, dysplastic features overlying epithelium accompanied by destruction of basement membrane. Underlying CT revealed keratin pearls & a superficial invasion of malignant cells in form of well-differentiated SCC, which had been restricted to nodules & did not spread to deeper areas. The striated muscle layer thickened & infiltration of inflammatory cells decreased noticeably. Tumor masses had been mostly replaced by proliferating fibrous tissue that had higher collagen deposition. In the 4 hamsters with severe dysplasia, the architectural and cytological dysplastic features included prominent nucleoli, cellular & nuclear pleomorphism, and hyperchromatism which extended more than two-thirds of epithelial thickness above the intact basement membrane Fig (4H). In 3 hamsters with moderate dysplasia, the dysplastic features extend two-thirds of epithelial thickness above the intact basement membrane. In hamsters with mild dysplasia, the dysplastic features extend up to one-third of epithelial thickness above the intact basement membrane. The mean DOI was 0.95mm. The IHC staining using ALDH1A1 exhibited mild positive cytoplasmic expression (mean = 7.7%) localized to basal & supra basal layers and scattered around peripheral cells of the tumor nests Fig. (6H).

3.3. Detection of apoptosis by (FCM)

The cell death was investigated for apoptotic activity using the annexin-V FITC/PI assay. Concerning apoptosis of all specimen cells, in untreated cells (GI), 3.6% of cells underwent apoptosis, while cells in GII (DMBA group) resulted in18.3% apoptosis. In treatment groups, GIII resulted in34.3% apoptosis, while GIV resulted in in27.1percent apoptosis, GV resulted in61.3% apoptosis, GVI resulted in 48.4% apoptosis, whereas cells in GVII resulted in 71.4 as shown in Fig. (7) and Table (10).

4. Discussion

With less than sixty percent of studied cases living to be older than five years, OSCC is a pathogenic kind of oral cancer that presents a serious health risk. Combination therapy is a multi-drug approach to cancer treatment. This strategy may improve therapeutic outcomes of cancer treatment while overcoming the drawbacks of monotherapy [30]. Current research uses the HBP system as an oral carcinogenesis model to evaluate efficacy of capecitabine in combination with salinomycin &/or GO nanoparticles. The evaluation had been based on gross observation, histological tumor tissue changes, IHC examination utilizing CSC marker ALDH1A1, and annexin V FITC/ PI staining assay using FCM. There were no discernible abnormalities in the GI gross observation in current research, gross observation outcomes in GI appeared no observable abnormalities. mucosa appeared pink in color with a smooth surface during experiment period. These findings agree with the studies that reported the same findings [31-32]. This result reflected on H & E staining which exposed that lining epithelium of HBP mucosa has been normally thin with3-5 cells thick keratinized stratified squamous epithelium. The basement membrane was intact with no rete processes. subepithelial CT, muscular layer & areolar CT had been seen normally. These findings agree with studies that reported the same findings [33-35]. These results may be due to the hamster not being exposed to the carcinogenic agent. Besides, about apoptosis of all cancer cells, FCM of apoptosis results in GI revealed 3.6% underwent apoptosis [36]. In this research, using IHC staining, GI revealed negative cytoplasmic expression of ALDH1A1 (mean = 4.1%). These results have been consistent with those reported by other investigators [37-39]. The expression had been limited to basal & supra basal layers, where the existence & activity of oral epithelial stem cells in basal cell layer are related to oral mucosa's high capacity for regeneration & rapid tissue replacement [40]. Due to the regular production of ALDHs in normal stem cells, which have been implicated in functioning of stem cells, such as proliferation, self-defense, differentiation, & preserving stemness in stem cells, ALDH1A1 activity is associated with stemness [41]. In current research, gross observation results in GII (DMBA treated group) exposed multiple exophytic nodules of variable size surrounded by an area of ulceration & bleeding, these tumor masses usually confluent and appear as large single mass (fungating tumor mass), general debilitation of animals, a significant decrease of pouches' length, hair loss, & skin lesions, corresponding with the outcomes of studies using same model [32,42]. This finding was corroborated by H & E staining, which revealed that DMBA-induced HBP tumors had been well to moderately differentiated SCC in form of papillomatous lesions with epithelial islands invading CT beneath. These outcomes agree with other research works [31,43]. According to other studies, 100% of tumors formed after 14weeks of painting DMBA alone on HBP showed well- & moderately-differentiated SCC, which is consistent with the findings of the current study [32-33,44-45]. This may be attributed to the pro-carcinogenic nature of DMBA, which induces the expression of cytochrome P 450 enzymes that metabolize DMBA into free radical intermediates, like superoxide, hydrogen peroxide, & nitrogen oxide, which could generate mutagenic DNA adduct through induction of oxidative stress and induce carcinogenesis [46]. Regarding apoptosis of all cancer cells, FCM of apoptosis results revealed 18.3% underwent apoptosis of a highly proliferative cancer tissue compared to GI. These findings concur with those of other studies [36, 47]. These outcomes may be attributed to the fact that apoptosis was observed to gradually increase from normal to dysplasia to OSCC because of large tumor size & aggressive biological behavior, tumor undergoes hypoxia leading to increased apoptosis. These attributions have been consistent with those described by Simila et al., (2018) [48]. In this research, using IHC staining, GII exposed moderate positive cytoplasmic expression (mean = 26.8%) during epithelial layers & cells of tumor nests and notably absent in the center of keratin pearls with highly significant expression (p-value < 0.001) compared to GI. Compatible finding was reported by other investigators [37, 39, 49]. Rao et al., (2020) revealed that increased ALDH1A1 expression is frequently noted in numerous cancers & is used as a CSC marker.

This increase in ALDH1A1 from oral epithelial dysplasia to OSCC could be attributed to role of ALDH in regulating several pathways that contribute to tumorigenesis & stem cell signaling. They have been primarily regulated by retinoic acid compounds & other oncogenic pathways like Wnt/β-catenin. ALDH1A1 oxidizes numerous aldehydes participating in different signaling mechanisms, minimizes ROS production, prevents DNA damage, & mediates retinoic acid signaling cascades. Numerous biological processes, including cellular proliferation, differentiation, oncogenesis, stemness, & resistance to chemotherapy & radiation, are impacted by these systems [41]. In the present research, Gross observation results in GIII presented marked reduction in size of exophytic masses as compared to GII with an area of bleeding in some animals, animals presented relative improvement in general health and there had been significant rise in pouch length in most of animals. This finding had been checked by H&E staining, which confirmed that 6 animals had well-differentiated SCC & 4 animals had severe dysplasia. These findings were in line with another study by Arjona-Sáncheza et al., (2010) [50]. These results could be described by the fact that capecitabine is a prodrug with a cytotoxic component that is specifically activated by tumors. Fluorodeoxyuridine monophosphate, which is produced when 5-FU is further broken down, binds to TS to create a ternary complex that is covalently bonded. This binding prevents uracil from becoming thymidylate. Lack of thymidylate may prevent cell division since it is a prerequisite for thymidine triphosphate, which is required to produce DNA and induces apoptosis [51-53]. This finding reflected on FCM of apoptosis, resulted in 34.3% apoptosis. There had been a highly statistically significant variation among GIII & GII regarding apoptosis (P-value < 0.001). These outcomes have been consistent with those reported by other investigators [54-56]. In the current research, using IHC staining, GIII demonstrated moderate positive cytoplasmic expression (mean = 41.1%) during epithelial layers & throughout cells of tumor nests and was notably absent in the center of keratin pearls. The result showed a highly significant expression (p-value < 0.001) compared to GI and GII. These outcomes did not differ much from other studies [57-59]. Cheo et al., (2020) demonstrate that 5-FU-based chemotherapy as capecitabine induces activation & enrichment of CSCs in residual tumors, contributing to recurrence after treatment. 5-FU-based chemotherapy activates CSCs by p53-induced Wnt3 transcription, which has been followed by activation of Wnt/β-catenin pathway in colorectal cancer cell lines & xenograft tumors [60]. Wang et al., (2014) evaluated expression of CD133, EMT & Wnt/β-catenin signaling pathway in tumors of mouse xenograft models, result showed that the expression of CD133 had been increased in5-FU group compared with the control group, 5-FU based chemotherapy-induced EMT by down-regulation of E-cadherin & up-regulation of vimentin expression, in addition to activation of Wnt/β-catenin signaling pathway induced by 5-FU [57]. Maintaining cancer stemness is aided by Wnt overexpression & the β-catenin nuclear localization that goes along with it. EMT has been marked by loss of E-cadherin protein, & overexpression of this pathway outcomes in highly invasive CSCs [61]. In this research, gross observation results in GIV exposed a slight reduction in size & number of exophytic masses as compared to GII but less than GIII, marked ulceration and exudates around mass surfaces were noticed and animals presented marked improvement in general health. This finding reflected on H & E staining in which only 7animals exhibited well-differentiated SCC & 3animals exhibited severe dysplasia. These outcomes have been consistent with those reported by other investigators [62-63]. These findings can be attributed to the anticancer effects of GO. Wang et al., (2020) found that GO prevented cervical cancer cells from migrating & invading [64]. Because GO therapy led to cytotoxicity, reactive ROS generation, apoptosis, autophagy, & activation of AMPK/mTOR/ULK1signal pathway, it greatly suppressed tumor growth both in vitro & in vivo [65]. In contrast to the findings of the present research, Zhu et al., (2019) showed that low-dose GO could enhance invasion/migration & alterations of representative EMT indicators inGO-treated cells resulting in improved lung metastasis of cancer cells in numerous metastasis models [66]. Latter was in line with Zheng Z et al (2023) showing that low-dose GO promotes tumor cell proliferation [67]. This discrepancy may be due to using low-dose GO that causes severe damage rather than high-dose GO. In addition, direct injection shows less toxicity than intravenous injection. The technique of GO production, the dose to be given, the administration route, & nanomaterial's physicochemical characteristics all affect how poisonous the material is [68-69]. Regarding to FCM of apoptosis, GIV resulted in 27.1% apoptosis. There had been a highly statistically significant variation between GIV & GII regarding apoptosis (P-value < 0.001). These outcomes have been consistent with those reported by other investigators [70-71]. Mousavi et al., (2022) revealed that GO-based nano therapy has an apoptotic effect in the OSCC cell line [72]. Krasteva et al., (2018) conclude that the cytotoxic impact of GO on cancer cells may be enhanced by generation of ROS, DNA damage, & apoptosis, hence considerably aiding in the death of cancer cells [73]. In the current research, using IHC staining, GIV showed mild positive cytoplasmic expression (mean = 17.4%) during epithelial layers & cells of tumor nests. The result showed a highly significant expression (p-value < 0.001) compared to GII. These outcomes did not differ much from other studies [20,74]. Wang et al., (2020) revealed usefulness of GO to inhibit growth & promote differentiation of CSCs, to suppress malignancy of glioblastoma [20]. Fiorillo et al., (2015) revealed that these results may be attributed to that by blocking several important signal transduction pathways, including WNT, Notch, & STAT-signaling, GO has a profound influence on CSCs by causing CSC differentiation. Therefore, using differentiation-based nano-therapy to eradicate CSCs, GO might be a useful non-toxic therapeutic approach. According to the latter research, GO may be utilized directly as a therapy to target CSCs, perhaps acting as a differentiating agent [75]. In the current research, Gross observation outcomes in GV revealed marked reduction in size & number of exophytic masses as compared to GII, GIII, and GIV with the absence of erosive, inflammation & bleeding surfaces around masses. This result reflected on H & E staining in which only 3animals exhibited well-differentiated SCC with the superficial invasion of malignant cells, 6animals exhibited severe dysplasia & 1 animal exhibited moderate dysplasia. These findings were by several studies [57, 76].

These results may be attributed to the chemotherapeutic effects of capecitabine and the anticancer effect of salinomycin by various mechanisms in different cancer types [77-80]. Moreover, a combination of salinomycin & capecitabine resulted in synergistic antitumor impact against liver tumors both in vitro & in vivo [57]. Latter was in line with Klose et al., (2019) who found that salinomycin in combination with5-FU exerts increased antitumoral activity in the pre-clinical colorectal cancer model compared to common chemotherapy [76]. Regarding to FCM of apoptosis, GV resulted in 61.3% apoptosis. There had been a highly statistically significant variation among GV & GII regarding apoptosis (P-value < 0.001) and there had been highly statistically significant variation among GV & GIII regarding apoptosis (P-value < 0.001). Based on results, Salinomycin in combination with capecitabine exerts increased antitumoral activity compared to common chemotherapy. By inhibiting P-gp, salinomycin may overcome drug resistance in human cancer cells & restore their sensitivity to chemotherapeutic agents [80-81]. By using FCM analysis to assess the combined effect of Sal & 5-FU on apoptotic effects, findings demonstrated that combination therapy markedly boosted apoptosis of hepatocellular carcinoma cell lines [57]. In this research, using IHC staining, GV revealed mild positive cytoplasmic expression (mean = 14.2%) localized to basal & supra basal layers & scattered around the peripheral cells of the tumor nests. The result showed a highly significant expression (p-value < 0.001) compared to the capecitabine-alone treated group (GIII). These results have been consistent with those reported by other investigators [61,74]. Sivanesan et al., (2021) revealed that salinomycin was effective in lowering stemness markers & EMT that are associated with 5-FU resistance [61]. A compatible finding was informed by Wang et al., (2014), who evaluated the expression of CD133 in tumors of mouse xenograft models by IHC, 5-FU combined with salinomycin decreased the proportion of CD133 compared with 5-FU treatment group. In the same research, salinomycin inhibited EMT by up-regulating expression of E-cadherin. Also, 5-FU combined with salinomycin determined that salinomycin altered EMT induced by 5-FU. Also, the findings showed that when compared to 5-FU alone, salinomycin alone & salinomycin plus 5-FU both down-regulated expression of active β-catenin. Findings showed that combination therapy changed how 5-FU activated Wnt/β-catenin signaling pathway [57]. In the current research, Gross observation outcomes in GVI revealed marked reduction in size & number of exophytic masses as compared to GII and GIII but less than GV. This finding reflected on H & E staining in which 5animals exhibited well-differentiated SCC superficial invasion of malignant cells, 4 animals exhibited severe dysplasia & 1 animal exhibited moderate dysplasia. Based on the results, GO paved new avenue to use as new class of chemosensitizer which could be potentially applied as adjuvant agents and strongly enhanced the sensitivity of chemotherapeutic agents to improve the effect of chemotherapy and overcome drug resistance of CSCs. Compatible findings were reported by other researchers [82-83]. Afarideh et al., (2018) presented significant inhibition of adenocarcinoma cells using GO/5-FUcompared to free 5-FU or GO alone [84]. Regarding to FCM of apoptosis, GVI resulted in 48.4% apoptosis. There had been highly statistically significant variation among GVI and GII, GIII & GVI regarding apoptosis (P-value < 0.001). Based on results, the rate of apoptosis significantly increased in cells after combination therapy of capecitabine and GO, compared to groups treated with capecitabine or GO alone. These outcomes did not differ much from those reported by Sanad et al., (2019) [85].

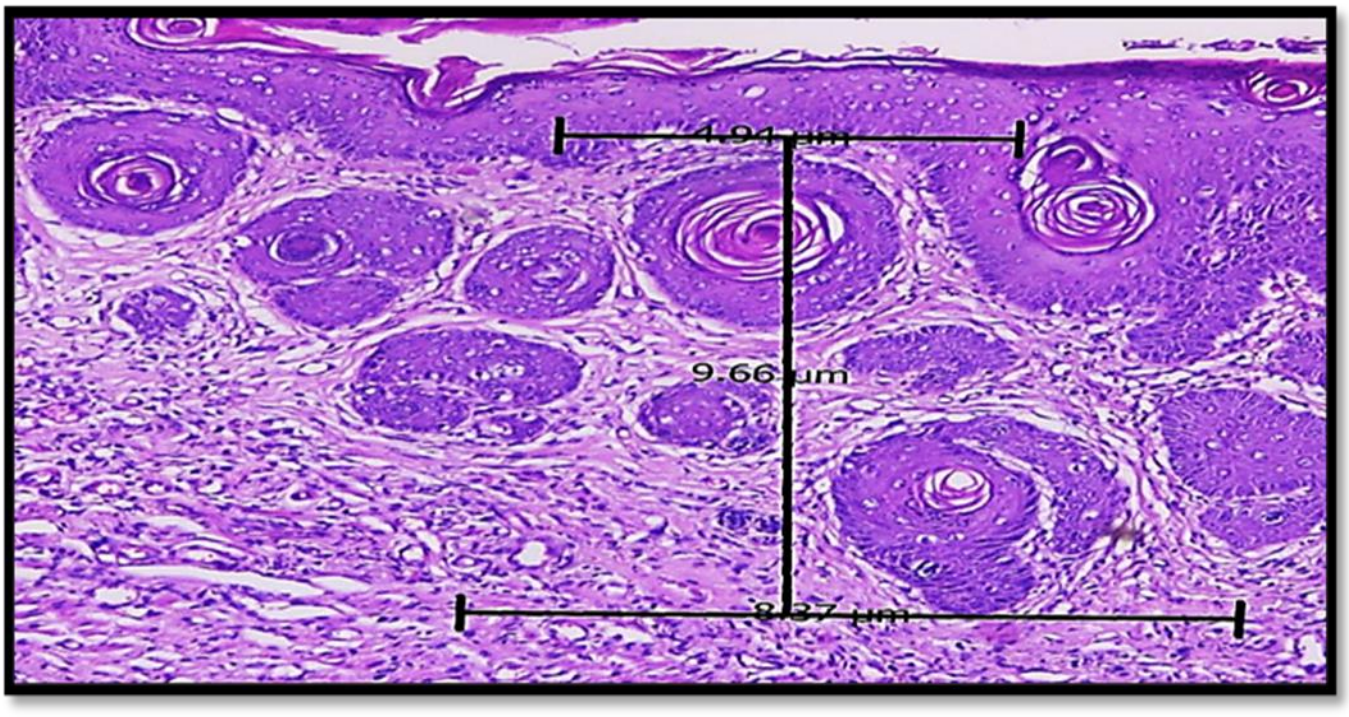

Figure 1: Photograph of measuring DOI, greatest invasion had been measured by dropping “plumb line” from horizon to deepest invasive nest.

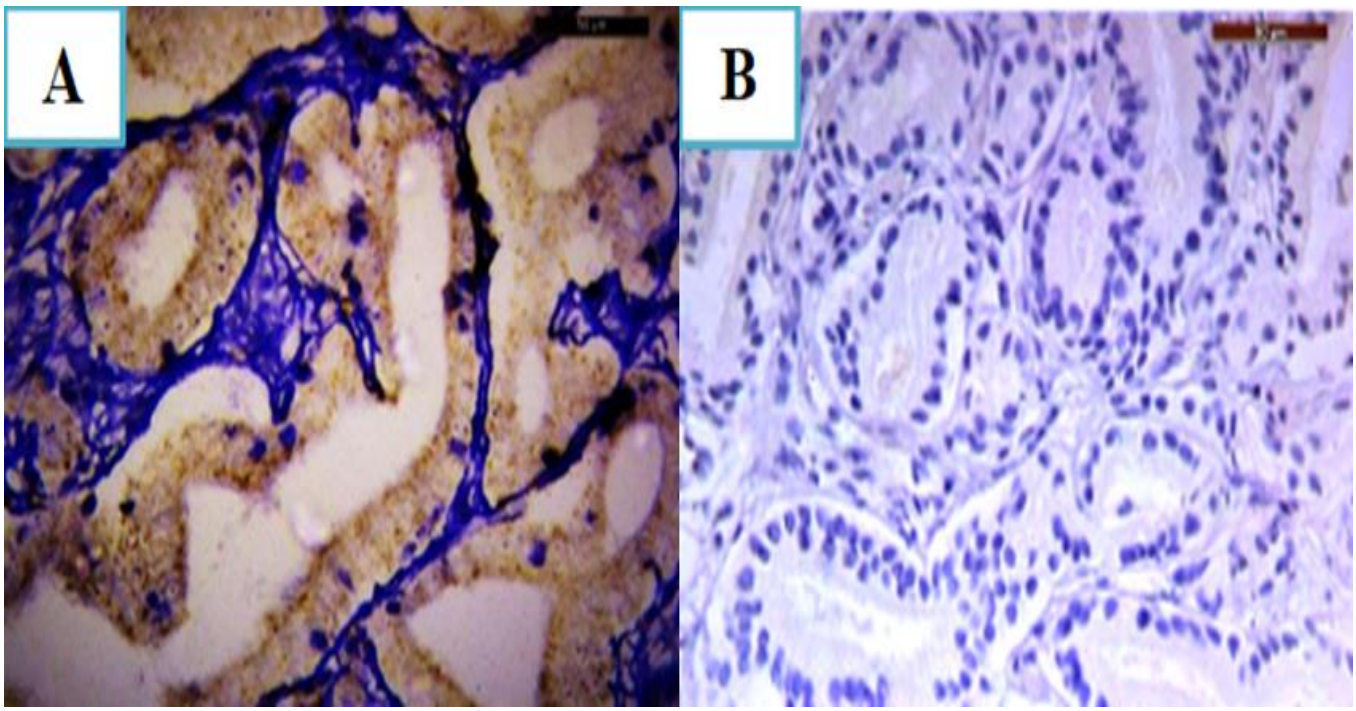

Figure 2: A: As a positive control, expression of ALDH1A1 antibody in prostate cancer tissue section showing positive cytoplasmic staining. **B**: As a negative control, the prostate tissue section shows negative expression.

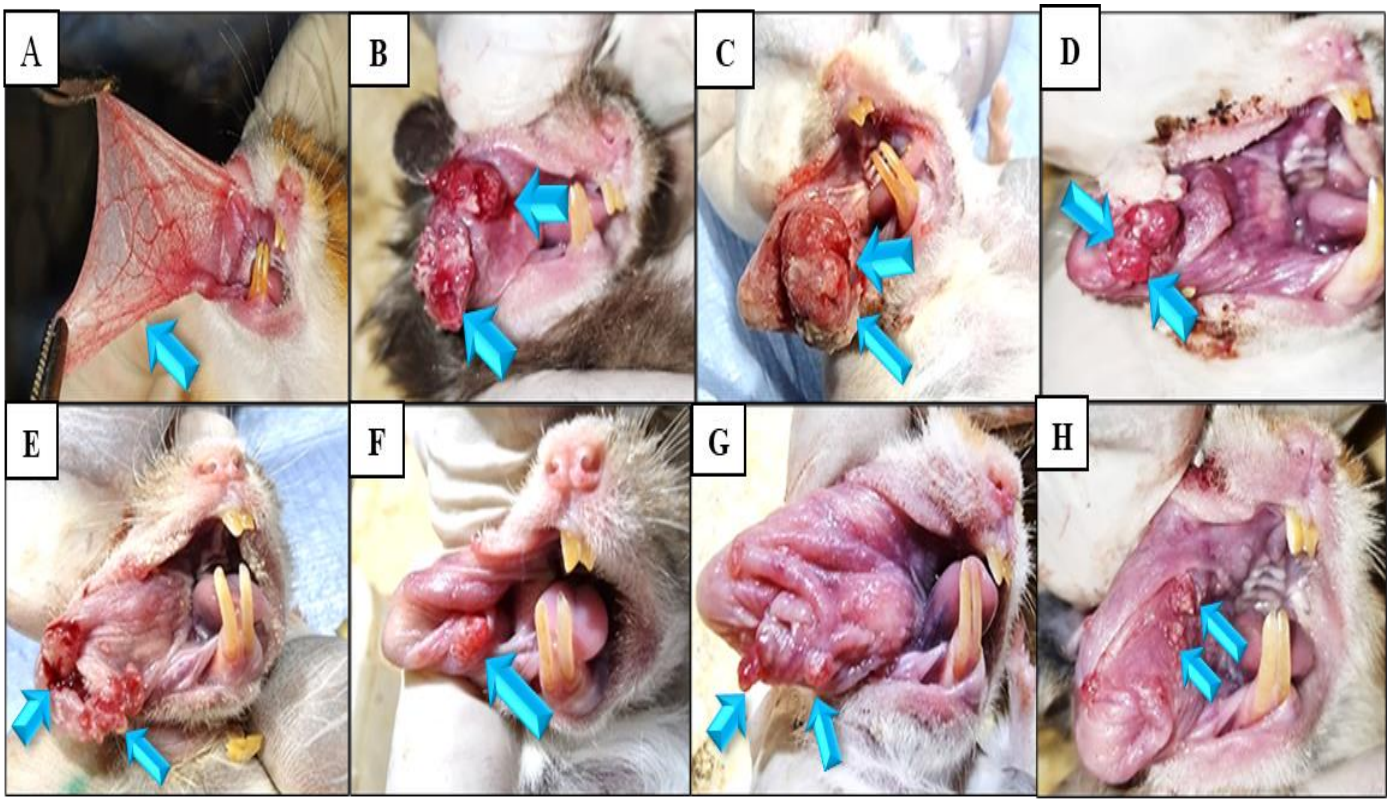

Figure 3: Gross observations: Fig. (3A): Photograph of GI indicating normal buccal pouch with normal mucosa (arrow). Fig. (3B): Photograph of GII indicating multiple large nodules (arrow) surrounded with an area of ulceration & bleeding (arrowhead). Fig. (3C): Photograph of GII indicating a single large nodule (fungating tumor mass) (arrow) surrounded with an area of bleeding (arrowhead) Fig. (3D): Photograph of GIII showing multiple exophytic masses with detectable nodular growth regression (arrow) and little bleeding and ulceration (arrow). Fig. (3E): Photograph of GIV indicating multiple exophytic masses (arrow) surrounded with bleeding & ulcerated areas (arrowhead). Fig. (3F): Photograph of GV indicating a detectable nodular growth regression (arrow) Fig. (3G): Photograph of GVI showing multiple nodules of a small size with little ulceration (arrows) Fig. (3H): Photograph of GVII showing multiple variable small nodules (arrows).

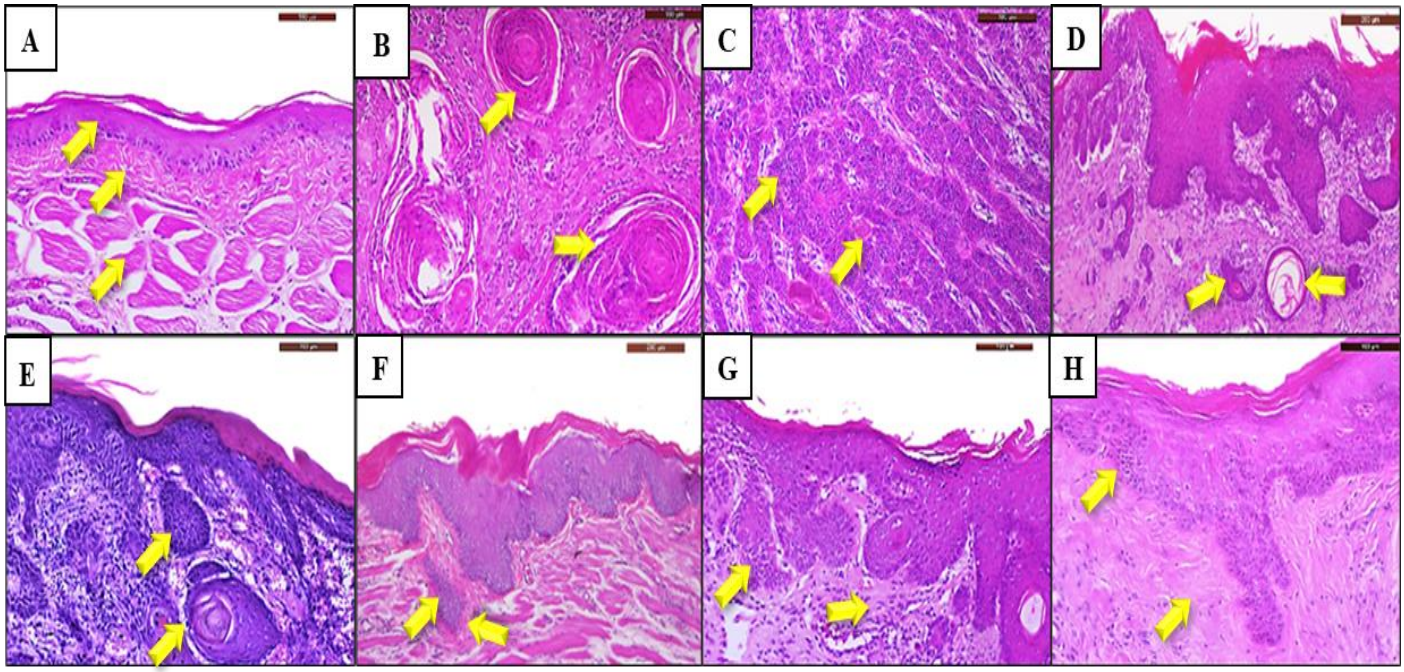

Figure 4: Gross observations & histopathological results: Fig. (4A): GI of HBP mucosa showing a well-defined layer of stratified squamous epithelium with flattened rete ridges (golden arrow), delicate & loose connective tissue (arrowhead) & layer of striated muscle fibers (red arrow) (H & E stain, x200). Fig. (4B): GII of HBP mucosa viewing well-differentiated SCC with deeply invasive epithelial nests & keratin pearls (arrow) (H & E stain, x 200). Fig. (4C) GII of HBP mucosa indicating moderate differentiated SCC composed of cords or islands of neoplastic atypical epithelial cells with less keratin formation (arrow) (H & E stain, x100) Fig. (4D): GIII of HBP mucosa indicating well-differentiated SCC with invading islands to the underlying CT which did not invade deeply into underlying CT & nests appeared less in size (arrows). Presence of fibrous tissue surrounding nests (arrowhead) (H & E stain, x100). Fig. (4E): GIV of HBP mucosa indicating well-differentiated SCC with invading islands to the underlying CT which did not invade deeply into underlying CT & nests appeared less in size (arrows). (H & E stain, x200). Fig. (4F): GV of HBP mucosa showing superficial invasive SCC and revealed residual small epithelial island (arrow). Presence of fibrous tissue surrounding nests (arrowhead) (H & E stain, x100). Fig. (4G): GIV of HBP mucosa showing superficial invasive SCC and revealed residual small epithelial islands (arrow). Presence of fibrous tissue surrounding nests (arrowhead) (H & E stain, x200). Fig. (4H): GVII of HBP mucosa showing severe epithelial dysplasia with some criteria of malignancy (arrow) collagen fibers in CT (arrowhead) (H & E stain, x200).

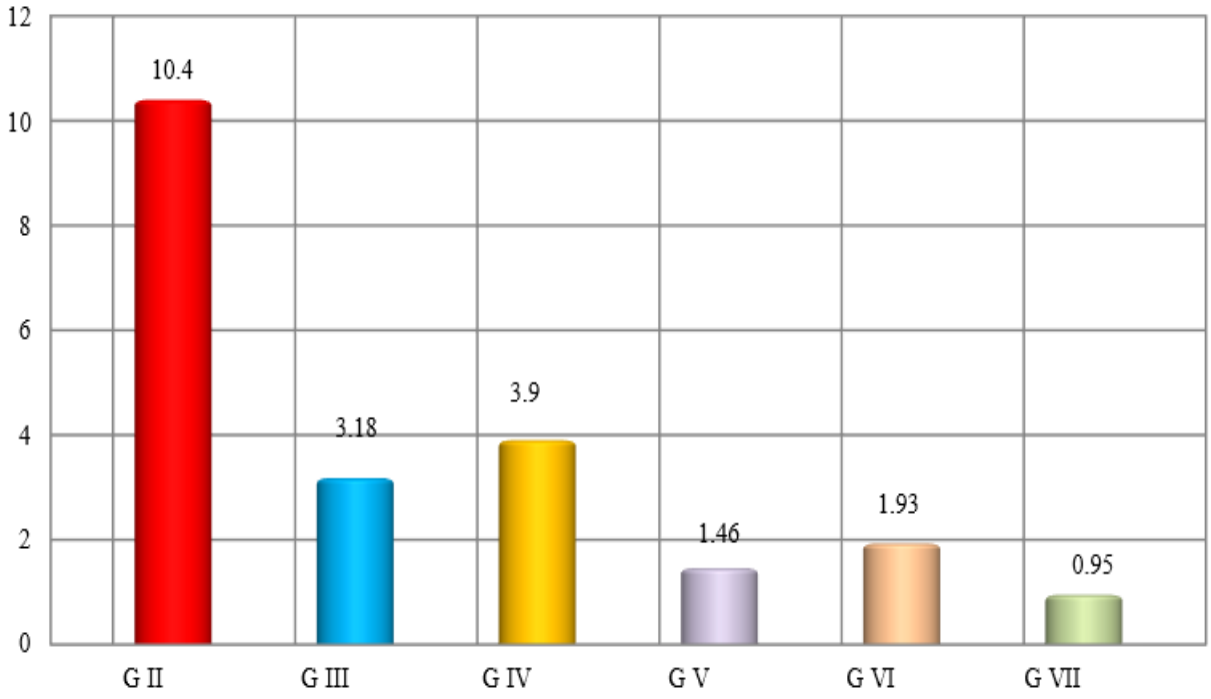

Figure 5: The bar chart represents a comparison among studied groups as regards DOI level.

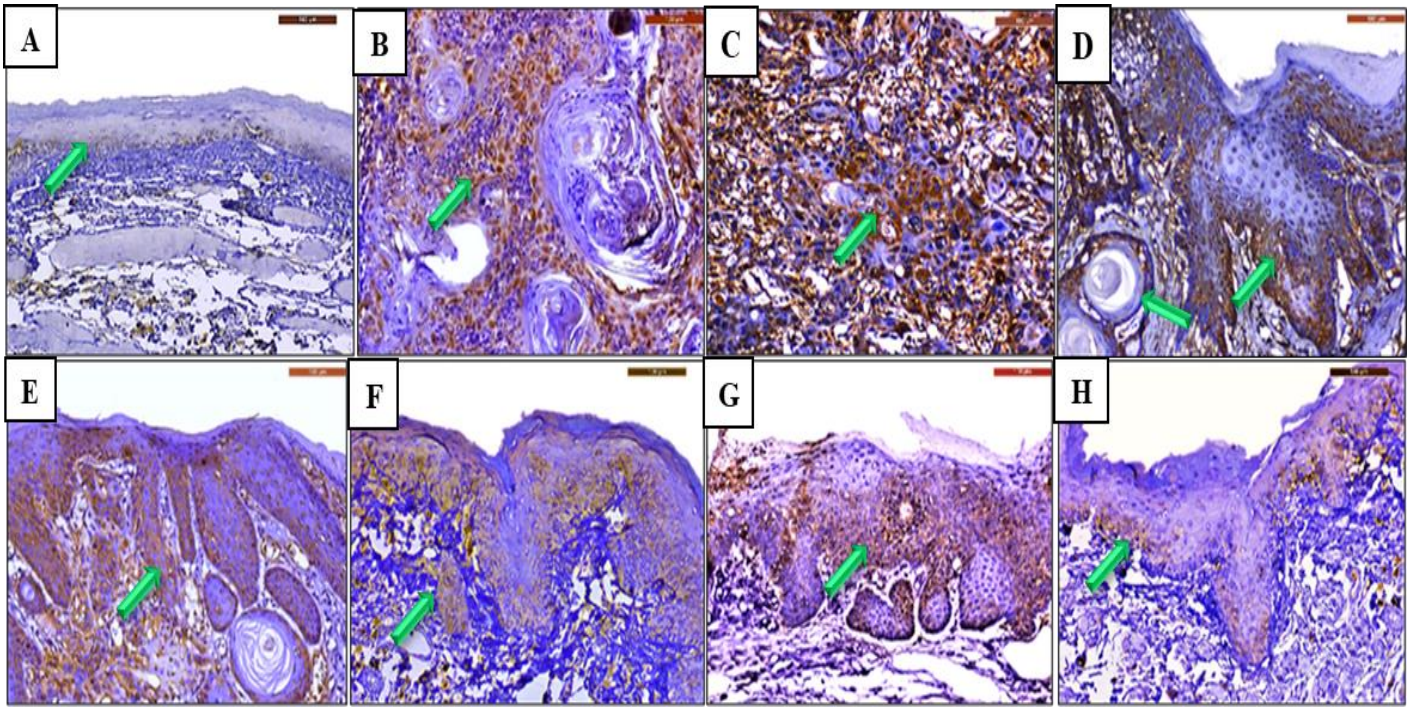

Figure 6: IHC outcomes: Fig. (6A): Expression of ALDH1A1 showing negative cytoplasmic expression in basal & supra basal epithelial layers (arrow) (Streptavidin biotin peroxidase, x200). Fig. (6B): Expression of ALDH1A1 indicating moderate positive cytoplasmic expression scattered during cells of tumor nests as brownish cytoplasmic staining and notably absent in the center of keratin pearls (arrow) (Streptavidin biotin peroxidase, x200). Fig. (6C): Expression of ALDH1A1 indicating moderate positive cytoplasmic expression scattered during cells of tumor nests (arrow) (Streptavidin biotin peroxidase, x200). Fig. (6D): Expression of ALDH1A1 indicating moderate positive cytoplasmic expression scattered or diffuse in cells of the tumor nests (arrows) (Streptavidin biotin peroxidase, x200). Fig. (6E): Expression of ALDH1A1 indicating mild positive cytoplasmic expression scattered in cells of tumor nests and scattered around the peripheral cells of the tumor nests (arrow) (Streptavidin biotin peroxidase, x200). Fig. (6F): Expression of ALDH1A1 indicating mild positive cytoplasmic expression localized to basal& supra basal layers & scattered around peripheral cells of the tumor nests (arrow) (Streptavidin biotin peroxidase, x200). Fig. (6G): Expression of ALDH1A1 indicating mild positive cytoplasmic expression localized to basal & supra basal layers & scattered around peripheral cells of the tumor nests (arrow) (Streptavidin biotin peroxidase, x200). Fig. (6H): Expression of ALDH1A1 indicating mild positive cytoplasmic expression localized to basal & supra basal layers (arrow) (Streptavidin biotin peroxidase, x200).

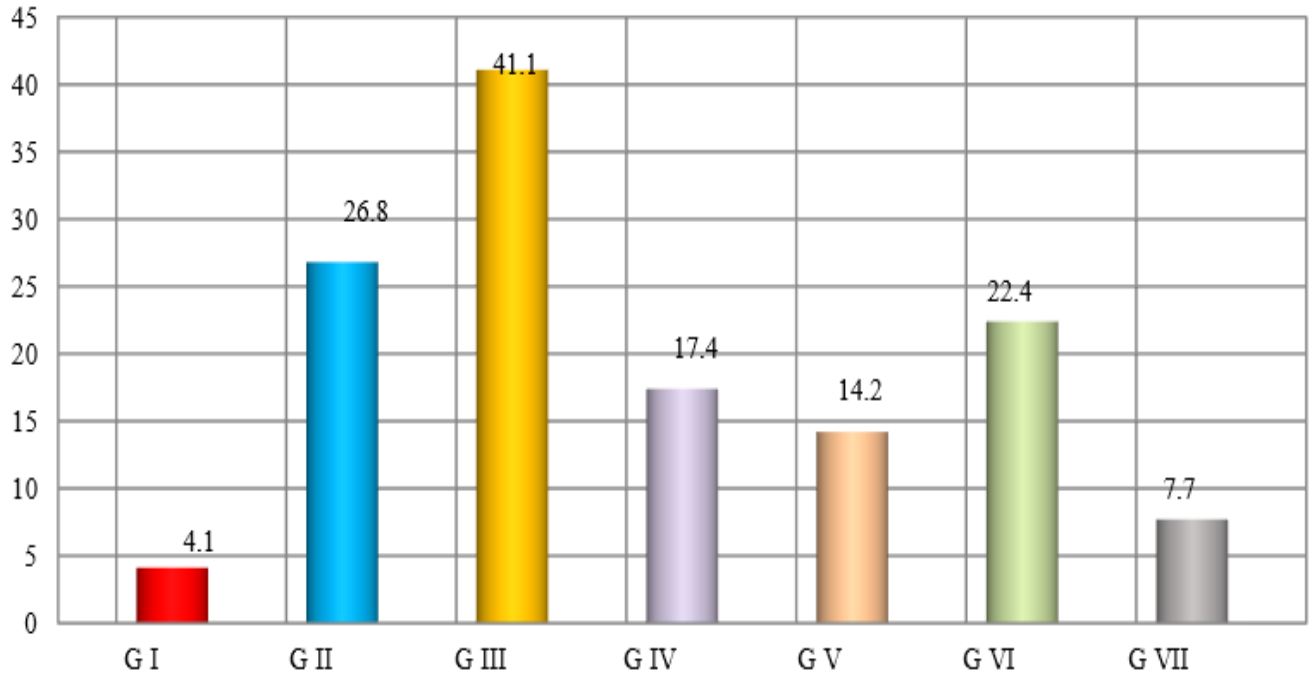

Figure 7: The bar chart represents a comparison between studied groups as regards ALDH1A1.

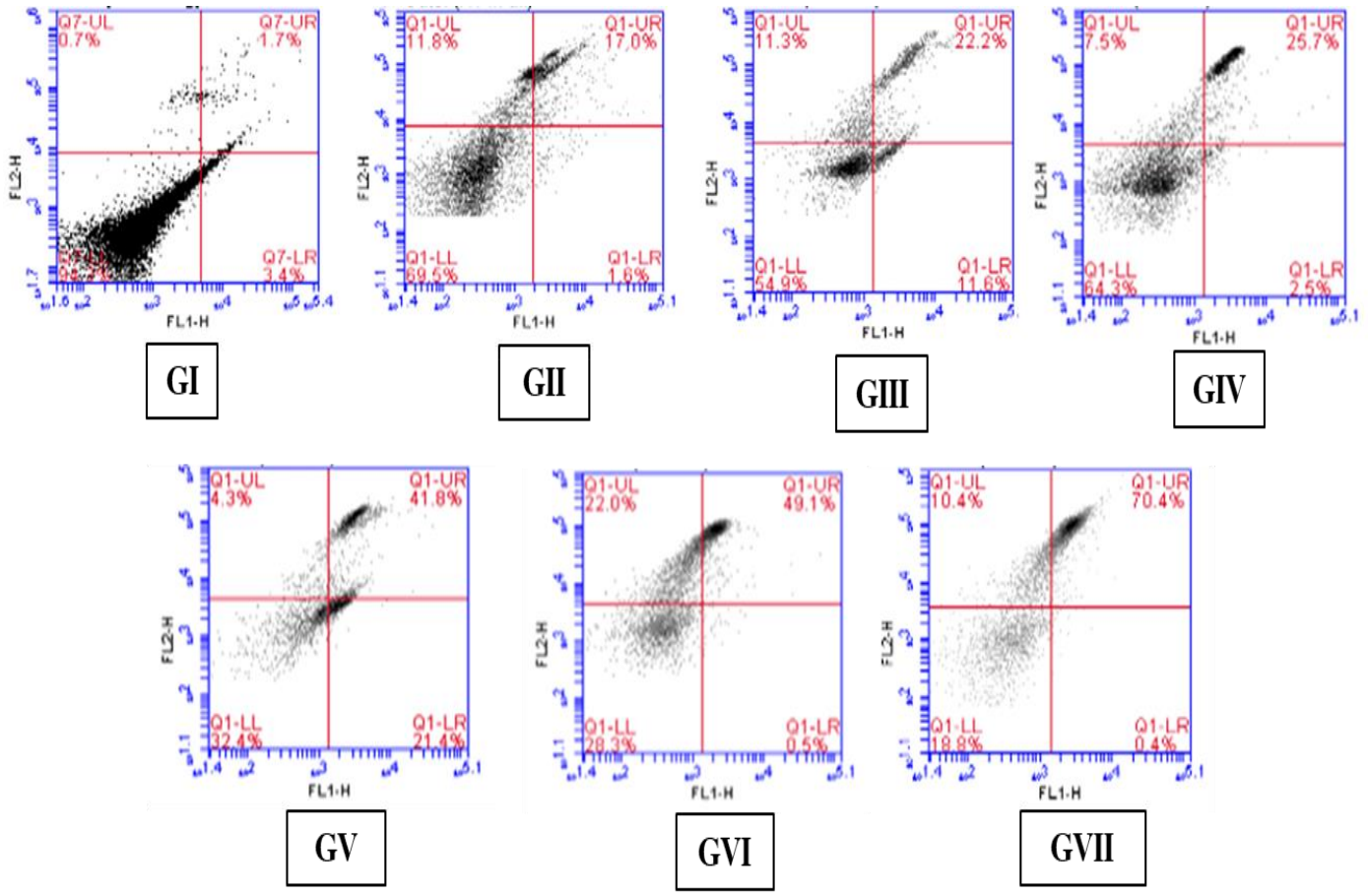

Figure 8: Scatterplots for detection apoptosis of GI, GII, GIII, GIV, GV, GVI & GVII.

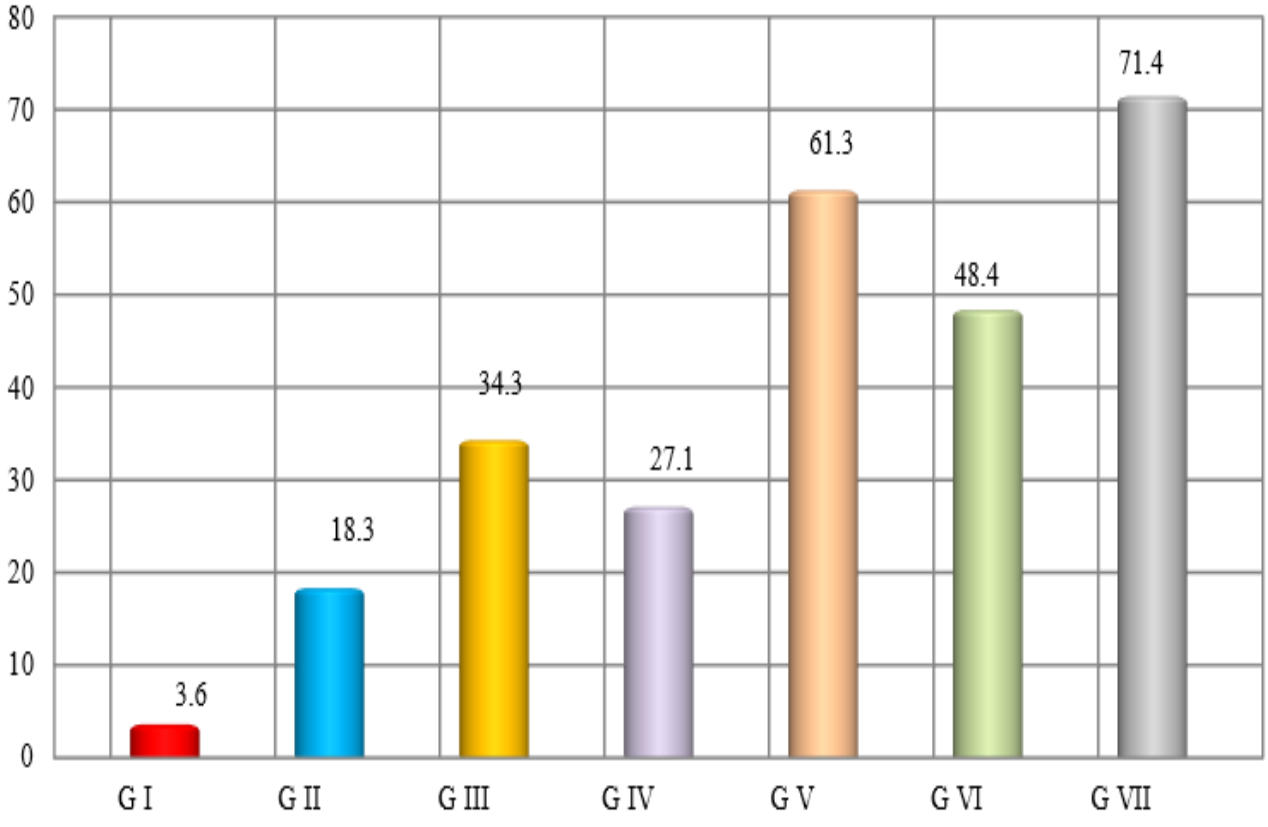

Figure 9: The bar chart represents a comparison between studied groups as regards Apoptosis %.

In the current research, using IHC staining, GVI revealed mild positive cytoplasmic expression (mean = 22.4%) localized to basal & supra basal layers and scattered around peripheral cells of the tumor nests. The result showed a highly significant expression compared to GIII (p-value < 0.001). The outcomes have been based on facts of effective non-toxic therapeutic strategy of GO for eradication of CSCs, by differentiation-based nano-therapy [75]. Combination with capecitabine promoted the killing of differentiated cancer cells. These results did not differ much from the study of Lin et al., (2018) that revealed a combination of GO & chemotherapeutic agents promoted the killing of colon cancer, ovarian, cervical, & prostate cancer cells [82]. In the current research, Gross observation findings in GVII confirmed various changes: rough whitish granular surface, mild erythema, and some tiny red exophytic lesions. There had been a significant reduction in the size of exophytic masses rather than other animals in this study with the absence of ulceration & bleeding. These results reflected on the H & E stain showed that 2 animals exhibited well-differentiated SCC with the superficial invasion of the malignant cells, 4 animals exhibited severe epithelial dysplasia, 3 animals exhibited moderate dysplasia & 1 animal exhibited mild dysplasia. Regarding to FCM of apoptosis, GVII resulted in 71.4% apoptosis. There had been a highly statistically significant variation among GVII & other medicated groups regarding apoptosis (P-value < 0.001). Based on the results, these combinatorial treatments strongly induced apoptosis. These results may be attributed to that each therapeutic agent has the potential for cancer therapy and induces apoptosis by different pathways. Besides, a combination of salinomycin & capecitabine resulted in synergistic antitumor effect against liver tumors both in vitro & in vivo [61]. Moreover, a combination of GO and salinomycin induced apoptosis 5-fold higher level than each treatment alone and sensitizing tumor cells [74]. In this study, using IHC staining, GVII revealed mild positive cytoplasmic expression (mean = 7.7%) localized to the basal and supra basal layers and weakly scattered around the peripheral cells of the tumor nests. The result showed a highly significant expression (p-value < 0.001) compared with GIII, GIV, GV, GVI, or GVII. The findings are predicated on the likelihood that therapeutic targeting of CSCs will be difficult since both bulk tumor cells & CSCs should be eradicated, possibly necessitating combined medication treatments. The previous results of using tri-therapeutic agents did not differ much from other studies that used three-drug combinations, the observed responses of these studies reveal significant enhancement and efficacy of cancer treatment [86-87]. Combination therapy is preferred over single-agent chemotherapy because of the synergistic effects of the combination therapy which can target multiple cancer signaling pathways, less toxicity, and due to the heterogeneity of tumors, there are increased chances for overcoming chemoresistance.

5. Conclusions

Combining three active cytotoxic agents including capecitabine, salinomycin, and GO improves anticancer efficacy by inhibiting growth and inducing apoptosis, targeting CSCs by differentiation or eradication, overcoming chemoresistance, and sensitizing tumor cells.

References

[1] S. Hegde, V. Ajila, W. Zhu, C. Zeng. (2022). Artificial intelligence in early diagnosis and prevention of oral cancer. Asia-Pacific Journal of Oncology Nursing. 9 (12): 100133.

[2] M. Bellantoni, G. Picciolo, I. Pirrotta, N. Irrera, M. Vaccaro, F. Vaccaro, F. Squadrito, G. Pallio. (2023). Oral cavity squamous cell carcinoma: an update of the pharma-cological treatment. Biomedicines. 11: (4): 1112.

[3] S. He, R. Chakraborty, S. Ranganathan. (2022). Proliferation and apoptosis pathways and factors in oral squamous cell carcinoma. International Journal of Molecular Sciences. 23 (3): 1562.

[4] A. D. Colevas. (2006). Chemotherapy options for patients with metastatic or recurrent squamous cell carcinoma of the head and neck. Journal of Clinical Oncology. 24 (17): 2644-2652.

[5] Z. J. Law, X. H. Khoo, P. T. Lim, B. H. Goh, L. C. Ming, W. L. Lee, H. P. Goh. (2021). Extracellular vesicle-mediated chemoresistance in oral squamous cell carcinoma. Frontiers in Molecular Biosciences. 8: 629888.

[6] Á. F. Morel, A. Hasanovic, A. Morin, C. Prunier, V. Magnone, K. Lebrigand, A. Aouad, S. Cogoluegnes, J. Favier, C. Pasquier, I. Mus-Veteau. (2022). Persistent properties of a subpopulation of cancer cells overexpressing the hedgehog receptor patched. Pharmaceutics. 14 (5): 988.

[7] S. Bisht, M. Nigam, S. Kunjwal, P. Sergey, A. Mishra, J. Sharifi-Rad. (2022). Cancer stem cells: from an insight into the basics to recent advances and therapeutic targeting. Stem Cells International, 2022.

[8] M. H. Amer, M. M. A. Hassan, F. M. Attia, K. A. El-nour, K. Mohamed, A. M. M. E. Korraah. (2020). XRCC1 immunohistochemical expression in DMBA-induced oral squamous cell carcinoma treated with different thymoquinone preparations. Dental Science Updates. 1 (2): 151-159.

[9] M. N. El-Mansy, M. M. Hassan, K. A. El-Nour, M. Kholoud, W. El-Hosary. (2017). Treatment of oral squamous cell carcinoma using thymoquinone loaded on gold nanoparticles. Suez Canal University Medical Journal. 20 (1): 11-19.

[10] M. Morales-Herrero, I. Ortega-Medina. (2022). Experimental carcinogenesis with 7,12- dimethyl benz(a)anthrazene (DMBA) and its inhibition with isothiocyanates. Journal of oral research. 11 (4): 1-13.

[11] X. Xi, X. Huang, H. Yuan, J. Ni, F. Yang. (2022). Efficacy of sequential capecitabine on adjuvant chemotherapy of triple-negative breast cancer. Journal of Healthcare Engineering, 2022.

[12] L. de Boo, K. Jóźwiak, H. Joensuu, H. Lindman, S. Lauttia, M. Opdam, C. van Steenis, W. Brugman, R. J. Kluin, P. C. Schouten, M. Kok. (2022). Adjuvant capecitabine-containing chemotherapy benefit and homologous recombination deficiency in early-stage triple-negative breast cancer patients. British Journal of Cancer. 126 (10): 1401-1409.

[13] L. Muratori, A. Salvia, G. Gorzegno, P. Sperone, G. V. Scagliotti. (2020). Long-term disease control in a metastatic squamous cell carcinoma of the oral cavity treated with maintenance metronomic capecitabine. Journal of Oncology Pharmacy Practice. 26 (1): 240-243.

[14] A. Palmer, P. Sorger. (2017). Combination cancer therapy can confer benefit via patient-to-patient variability without drug additivity or synergy. Cell. 171 (7): 1678-1691.

[15] V. Soni, A. Nagar, R. Bardiya, J. Mara, L. V. Suskil, S. Rose, C. Sonawane. (2023). A concise review of prodigious salinomycin and its derivatives effective in treatment of breast cancer: (2012–2022). International Journal of Translational Medicine. 3 (2): 217-245.

[16] M. Antoszczak. (2019). A comprehensive review of salinomycin derivatives as potent anticancer and anti-CSCs agents. European Journal of Medicinal Chemistry. 166: 48-64.

[17] H. Wang, H. Zhang, Y. Zhu, Z. Wu, C. Cui, F. Cai. (2021). Anticancer mechanisms of salinomycin in breast cancer and its clinical applications. Frontiers in oncology. 11: 654428.

[18] J. Jiang, H. Li, E. Qaed, J. Zhang, Y. Song, R. Wu, X. Bu, Q. Wang, Z. Tang. (2018). Salinomycin, as an autophagy modulator- a new avenue to anticancer: a review. Journal of Experimental & Clinical Cancer Research. 37: 1-13.

[19] M. Maleki, R. Zarezadeh, M. Nouri, A. R. Sadigh, F. Pouremamali, Z. Asemi, H. S. Kafil, F. Alemi, B. Yousefi. (2020). Graphene oxide: A promising material for regenerative medicine and tissue engineering. Biomolecular Concepts. 11 (1): 182-200.

[20] X. Wang, W. Zhou, X. Li, J. Ren, G. Ji, J. Du, W. Tian, Q. Liu, A. Hao. (2020). Graphene oxide suppresses the growth and malignancy of glioblastoma stem cell-like spheroids via epigenetic mechanisms. Journal of Translational Medicine. 18: 1-14.

[21] Z. Cheng, M. Li, R. Dey, Y. Chen. (2021). Nanomaterials for cancer therapy: current progress and perspectives. Journal of hematology & oncology. 14: 1-27.

[22] M. Rose, J. Everitt, H. Hedrich, J. Schofield, M. Dennis, E. Scott, G. Griffin. (2013). ICLAS Working group on harmonization: International guidance concerning the production care and use of genetically-altered animals. Laboratory Animals. 47 (3): 146-152.

[23] A. Vinoth, R. Kowsalya. (2018). Chemopreventive potential of vanillic acid against 7,12 dimethylbenz-(a)anthracene-induced hamster buccal pouch carcinogenesis. Journal of Cancer Research and Therapeutics. 14 (6): 1285-1290.

[24] S. Anand, A. Yasinchak, T. Bullock, M. Govande, E. Maytin. (2019). A non-toxic approach for treatment of breast cancer and its metastases: capecitabine enhanced photodynamic therapy in a murine breast tumor model. Journal of Cancer Metastasis and Treatment. 5: 1-14.

[25] J. Wu, Z. Li, Y. Yong, A. A. Pettitt, F. Zhou. (2018). Photothermal effects of reduced graphene oxide on pancreatic cancer. Technology in Cancer Research & Treatment. 17: 1533034618768637.

[26] D. Wu, Y. Zhang, J. Huang, Z. Fan, F. Shi, S. Wang. (2014). Salinomycin inhibits proliferation and induces apoptosis of human nasopharyngeal carcinoma cell in vitro and suppresses tumor growth in vivo. Biochemical and biophysical research communications. 443 (2): 712-717.

[27] M. Faisal, M. A. Bakar, A. Sarwar, M. Adeel, F. Batool, K. I. Malik, A. Jamshed, R. Hussain. (2018). Depth of invasion (DOI) as a predictor of cervical nodal metastasis and local recurrence in early-stage squamous cell carcinoma of oral tongue (ESSCOT). PLoS One. 13 (8): 0202632-0202642.

[28] W. T. Liu, W. B. Liu, M. Gao, Y. Y. Zhang, K. S. Gu. (2019). Expression of aldh1a1 and cd133 is associated with the prognosis and effect of different chemotherapeutic regimens in gastric cancer. Oncology letters. 18 (5): 4573-4582.

[29] B. Tribukait. (1984). Clinical DNA flow cytometry. Medical Oncology and Tumor Pharmacotherapy. 1: 211-218.

[30] R. G. Mostafa, E. S. Abd-El-Hamid, A. H. M. El-Bolok, E. A. Eldin, S. M. Tohamy. (2020). Combined effect of doxorubicin and pyrogallol on tongue squamous cell carcinoma SCC-25 Cells, an in vitro Study. Systematic Reviews in Pharmacy. 11 (10).

[31] V. Balakrishnan, S. Ganapathy, V. Veerasamy, R. Duraisamy, V. A. Sathiavakoo, V. Krishnamoorthy, V. Lakshmanan. (2022). Anticancer and antioxidant profiling effects of nerolidol against DMBA induced oral experimental carcinogenesis. Journal of Biochemical and Molecular Toxicology. 36 (6): e23029.

[32] W. Zhang, G. Yin, J. Dai, Y. Sun, R. M. Hoffman, Z. Yang, Y. Fan. (2017). Chemoprevention by quercetin of oral squamous cell carcinoma by suppression of the NF-κB signaling pathway in DMBA-treated hamsters. Anticancer Research. 37 (8): 4041-4049.

[33] R. Priyadarsini, N. Kumar, I. Khan, P. Thiyagarajan, P. Kondaiah, S. Nagini. (2012). Gene expression signature of DMBA-induced hamster buccal pouch carcinomas: modulation by chlorophyllin and ellagic acid. PLoS ONE. 7 (4): e34628.

[34] Y. Gan, A. E. He, L. Zhu, Y. Yao, L. Chunhua. (2022). Lycorine impedes 7,12 dimethylbenz(a)anthracene exposed hamster oral carcinogenesis through P13K/Akt and NF-κB inhibition. Turkish Journal of Biochemistry. 479 (6): 802-810.

[35] V. Vinothkumar, S. Manoharan. (2011). Chemo preventive efficacy of geraniol against 7,12-dimethylbenz[a]anthracene- induced hamster buccal pouch carcinogenesis. Redox Report. 16 (3): 91-100.

[36] M. M. Saleh, Z. E. Darwish, M. I. El Nouaem, G. M. Mourad, O. R. Ramadan. (2020). Chemo-preventive effect of green tea and curcumin in induced oral squamous cell carcinoma: an experimental study. Alexandria Dental Journal. 45 (3): 74-80.

[37] V. Gupta, M. K. Maurya, P. Agarwal, M. Kumar, M. Sagar, S. Raghuvanshi, S. Gupta. (2022). Expression of aldehyde dehydrogenase 1A1 in oral squamous cell carcinoma and its correlation with clinicopathological parameters. National Journal of Maxillofacial Surgery. 13 (2): 208-215.

[38] H. Kato, K. Izumi, T. Saito, H. Ohnuki, M. Terada, Y. Kawano, K. Nozawa-Inoue, C. Saito, T. Maeda. (2013). Distinct expression patterns and roles of aldehyde dehydrogenases in normal oral mucosa keratinocytes: differential inhibitory effects of a pharmacological inhibitor and RNAi-mediated knockdown on cellular phenotype and epithelial morphology. Histochemistry and cell biology. 139: 847-862.

[39] N. Ota, J. Ohno, K. Seno, K. Taniguchi, S. Ozeki. (2014). In vitro and in vivo expression of aldehyde dehydrogenase 1 in oral squamous cell carcinoma. International Journal of Oncology. 44 (2): 435-442.

[40] C. Fukumoto, D. Uchida, H. Kawamata. (2022). Diversity of the origin of cancer stem cells in oral squamous cell carcinoma and its clinical implications. Cancers. 14: 1-12.

[41] N. Swain, M. Thakur, J. Pathak, S. Patel, R. Hosalkar. (2022). Aldehyde dehydrogenase 1: Its key role in cell physiology and oral carcinogenesis. Dental and Medical Problems. 59 (4): e629-e635.

[42] B. D. A. Martínez, P. A. Barato Gómez, C. A. Iregui Castro, J. E. Rosas Pérez. (2020). DMBA-induced oral carcinoma in syrian hamster: increased carcinogenic effect by dexamethasone coexposition. BioMed Research International.

[43] D. Rajasekaran, S. Manoharan, M. M. Prabhakar, A. Manimaran. (2015). Enicostemma littorale prevents tumor formation in 7, 12-dimethylbenz (a) anthracene-induced hamster buccal pouch carcinogenesis. Human & experimental toxicology. 34 (9): e911-e921.

[44] M. Liu, C. Wen, S. Pan. (2021). Modulator effect of mangiferin on biochemical characterization in 7, 12-dimethylbenz [a] anthracene induced oral cancer in experimental hamsters. Veterinary Medicine and Science. 7 (5): e2015-e2025.

[45] A. V. Mariadoss, S. Kathiresan, R. Muthusamy, S. Kathiresan. (2013). Protective effects of [6]-paradol on histological lesions and immunohistochemical gene expression in DMBA induced hamster buccal pouch carcinogenesis. Asian Pacific Journal of Cancer Prevention. 14 (5): e3123-e3129.

[46] Y. J. Kwon, D. J. Ye, H. S. Baek, Y. J. Chun. (2018). 7, 12-Dimethylbenz [α] anthracene increases cell proliferation and invasion through induction of Wnt/β-catenin signaling and EMT process. Environmental toxicology. 33 (7): e729-e742.

[47] S. Nambiar, V. Hegde. (2016). Apoptosis in oral epithelial dysplastic lesions and oral squamous cell carcinoma: A prognostic marker. Indian Journal of Pathology and Microbiology. 59 (3): e284-e286.

[48] A. Simila, I. Joseph, T. Prasanth, L. Girish. (2018). Quantitative analysis of apoptotic cells in normal mucosa, oral epithelial dysplasia and oral squamous cell carcinoma using methyl green pyronin stain. International Journal of Health Sciences and Research. 8 (9): e52-e56.

[49] R. S. Rao, K. L. Raju, D. Augustine, S. Patil. (2020). Prognostic significance of ALDH1, Bmi1, and OCT4 expression in oral epithelial dysplasia and oral squamous cell carcinoma. Cancer Control. 27 (1): e1073274820904959.

[50] Á. Arjona-Sánchez, J. Ruiz-Rabelo, M. D. Perea, R. Vázquez, A. Cruz, M. D. C. Munoz, F. J. Padillo. (2010). Effects of capecitabine and celecoxib in experimental pancreatic cancer. Pancreatology. 10 (5): e641-e647.

[51] D. B. Longley, D. P. Harkin, P. G. Johnston. (2003). 5-fluorouracil: mechanisms of action and clinical strategies. Nature reviews cancer. 3 (5): e330-e338.

[52] M. Wisniewska-Jarosinska, T. Sliwinski, J. Kasznicki, D. Kaczmarczyk, R. Krupa, K. Bloch, A. Morawiec-Sztandera. (2011). Cytotoxicity and genotoxicity of capecitabine in head and neck cancer and normal cells. Molecular biology reports. 38 (1): e3679-e3688.

[53] İ. Suat Övey, Y. Güler. (2020). Apoptotic efficiency of capecitabine and 5-fluorouracil on human cancer cells through TRPV1 channels. Indian Journal of Biochemistry and Biophysics (IJBB). 57 (1): e64-e72.

[54] J. J. Zhu, J. J. Shan, L. B. Sun, W. S. Qiu. (2015). Study of the radiotherapy sensitization effects and mechanism of capecitabine (Xeloda) against non-small-cell lung cancer cell line A549. Genetics and Molecular Research. 14 (4): e16386-e16391.

[55] M. Li, N. Zhang, M. Li. (2017). Capecitabine treatment of HCT-15 colon cancer cells induces apoptosis via mitochondrial pathway. Tropical Journal of Pharmaceutical Research. 16 (7): e1529-e1536.

[56] G. Bellone, A. Carbone, V. Busso, T. Scirelli, A. Buffolino, C. Smirne, G. Emanuelli. (2006). Antagonistic interactions between gemcitabine and 5-fluorouracil in the human pancreatic carcinoma cell line Capan-2. Cancer biology & therapy. 5 (10): e1294-e1303.

[57] J. Shi, J. Li, H. Guan, W. Cai, X. Bai, X. Fang, X. Zhu. (2014). Anti-fibrotic actions of interleukin-10 against hypertrophic scarring by activation of PI3K/AKT and STAT3 signaling pathways in scar-forming fibroblasts. PloS one. 9 (5): e98228.

[58] P. Jiménez, E. Chueca, M. Arruebo, M. Strunk, E. Solanas, T. Serrano, Á. Lanas. (2017). CD24 expression is increased in 5-fluorouracil-treated esophageal adenocarcinoma cells. Frontiers in Pharmacology. 8 (1): e321.

[59] Z. Y. Xu, J. N. Tang, H. X. Xie, Y. A. Du, L. Huang, P. F. Yu, X. D. Cheng. (2015). 5-Fluorouracil chemotherapy of gastric cancer generates residual cells with properties of cancer stem cells. International journal of biological sciences. 11 (3): e284.

[60] Y. H. Cho, E. J. Ro, J. S. Yoon, T. Mizutani, D. W. Kang, J. C. Park, K. Y. Choi. (2020). 5-FU promotes stemness of colorectal cancer via p53-mediated WNT/β-catenin pathway activation. Nature communications. 11 (1): e5321.

[61] D. Sivanesan, R. P. Arun, R. S. Verma. (2021). Effect of salinomycin on EMT and stemness pathways in 5-FU-resistant breast cancer. Advances in Cancer Biology-Metastasis. 1 (1): e100004.

[62] D. Batiuskaite, N. Grinceviciute, V. Snitka. (2015). Impact of graphene oxide on viability of Chinese hamster ovary and mouse hepatoma MH-22A cells. Toxicology in Vitro. 29 (5): e1195-e1200.

[63] R. F. de Paula, I. A. Rosa, I. F. Gafanhão, J. L. Fachi, A. M. G. Melero, A. O. Roque, E. C. de Oliveira. (2020). Reduced graphene oxide, but not carbon nanotubes, slows murine melanoma after thermal ablation using LED light in B16F10 lineage cells. Nanomedicine: Nanotechnology, Biology and Medicine. 28 (1): e102231.

[64] J. Wang, P. Wang, Y. He, X. Liu, S. Wang, C. Ma, X. Wu. (2020). Graphene oxide inhibits cell migration and invasion by destroying actin cytoskeleton in cervical cancer cells. Aging (Albany NY). 12 (17): e17625.

[65] J. Shen, J. Dong, F. Shao, J. Zhao, L. Gong, H. Wang, Y. Cai. (2022). Graphene oxide induces autophagy and apoptosis via the ROS-dependent AMPK/mTOR/ULK-1 pathway in colorectal cancer cells. Nanomedicine. 17 (9): e591-e605.

[66] J. Zhu, B. Li, M. Xu, R. Liu, T. Xia, Z. Zhang, S. Liu. (2019). Graphene oxide promotes cancer metastasis through associating with plasma membrane to promote TGF-β signaling-dependent epithelial–mesenchymal transition. ACS nano. 14 (1): e818-e827.

[67] Z. Zheng, A. Halifu, J. Ma, L. Liu, Q. Fu, B. Yi, J. Zhu. (2023). Low-dose graphene oxide promotes tumor cells proliferation by activating PI3K-AKT-mTOR signaling via cellular membrane protein integrin αV. Environmental Pollution. 330 (1): e121817.

[68] A. Rhazouani, H. Gamrani, M. El Achaby, K. Aziz, L. Gebrati, M. S. Uddin, F. Aziz. (2021). Synthesis and toxicity of graphene oxide nanoparticles: A literature review of in vitro and in vivo studies. BioMed Research International.

[69] C. Fu, T. Liu, L. Li, H. Liu, Q. Liang, X. Meng. (2015). Effects of graphene oxide on the development of offspring mice in lactation period. Biomaterials. 40 (1): e23-e31.

[70] Z. Tang, L. Zhao, Z. Yang, Z. Liu, J. Gu, B. Bai, H. Yang. (2018). Mechanisms of oxidative stress, apoptosis, and autophagy involved in graphene oxide nanomaterial anti-osteosarcoma effect. International Journal of Nanomedicine. 1 (1): e2907-e2919.

[71] T. A. Tabish, M. Z. I. Pranjol, F. Jabeen, T. Abdullah, A. Latif, A. Khalid, S. Zhang. (2018). Investigation into the toxic effects of graphene nanopores on lung cancer cells and biological tissues. Applied Materials Today. 12 (1): e389-e401.

[72] S. M. Mousavi, S. A. Hashemi, Y. Ghahramani, R. Azhdari, K. Yousefi, A. Gholami, W. H. Chiang. (2022). Antiproliferative and apoptotic effects of graphene oxide@ AlFu MOF based saponin natural product on OSCC line. Pharmaceuticals. 15 (9): e1137.

[73] N. Krasteva, M. Keremidarska-Markova, K. Hristova-Panusheva, T. Andreeva, G. Speranza, D. Wang, M. Georgieva. (2019). Aminated graphene oxide as a potential new therapy for colorectal cancer. Oxidative medicine and cellular longevity.

[74] Y. J. Choi, S. Gurunathan, J. H. Kim. (2018). Graphene oxide–silver nanocomposite enhances cytotoxic and apoptotic potential of salinomycin in human ovarian cancer stem cells (OvCSCs): a novel approach for cancer therapy. International journal of molecular sciences. 19 (3): e710.

[75] M. Fiorillo, A. F. Verre, M. Iliut, M. Peiris-Pagés, B. Ozsvari, R. Gandara, M. P. Lisanti. (2015). Graphene oxide selectively targets cancer stem cells, across multiple tumor types: implications for non-toxic cancer treatment, via "differentiation-based nano-therapy". Oncotarget. 6 (6): e3553.

[76] J. Klose, S. Trefz, T. Wagner, L. Steffen, A. Preißendörfer Charrier, P. Radhakrishnan, M. Schneider. (2019). Salinomycin: Anti-tumor activity in a pre-clinical colorectal cancer model. PLoS One. 14 (2): e0211916.

[77] D. Meulendijks, L. Dewit, N. B. Tomasoa, H. Van Tinteren, J. H. Beijnen, J. H. M. Schellens, A. Cats. (2014). Chemoradiotherapy with capecitabine for locally advanced anal carcinoma: an alternative treatment option. British journal of cancer. 111 (9): e1726-e1733.

[78] R. Dada, M. El Sayed, J. Zekri. (2017). Neoadjuvant chemotherapy with capecitabine plus cisplatin in patients with locally advanced nasopharyngeal cancer: case series study. Journal of Global Oncology. 3 (5): e455-e458.

[79] S. Z. Kuo, K. J. Blair, E. Rahimy, A. Kiang, E. Abhold, J. B. Fan, W. M. Ongkeko. (2012). Salinomycin induces cell death and differentiation in head and neck squamous cell carcinoma stem cells despite activation of epithelial-mesenchymal transition and Akt. BMC cancer. 12 (1): e1-e14.

[80] J. Dewangan, S. Srivastava, S. K. Rath. (2017). Salinomycin: A new paradigm in cancer therapy. Tumor Biology. 39 (3): e1010428317695035.

[81] D. Qi, Y. Liu, J. Li, J. H. Huang, X. Hu, E. Wu. (2022). Salinomycin as a potent anticancer stem cell agent: State of the art and future directions. Medicinal research reviews. 42 (3): e1037-e1063.

[82] K. C. Lin, M. W. Lin, M. N. Hsu, G. Yu-Chen, Y. C. Chao, H. Y. Tuan, Y. C. Hu. (2018). Graphene oxide sensitizes cancer cells to chemotherapeutics by inducing early autophagy events, promoting nuclear trafficking and necrosis. Theranostics. 8 (9): e2477.

[83] B. D. Biosciences. (2011). Detection of Apoptosis Using the BD Annexin V FITC Assay on the BD FACSVerse™ System.

[84] B. Afarideh, M. Rajabibazl, M. Omidi, B. Yaghmaee, A. Rahimpour, R. Khodabakhshi, S. Sarvarian. (2018). Anticancer activity of graphene oxide/5-FU on CT26 Ds-Red adenocarcinoma cell line. Oriental Journal of Chemistry. 34 (4): e2002.

[85] M. F. Sanad, A. E. Shalan, S. M. Bazid, E. S. A. Serea, E. M. Hashem, S. Nabih, M. A. Ahsan. (2019). A graphene gold nanocomposite-based 5-FU drug and the enhancement of the MCF-7 cell line treatment. RSC advances. 9 (53): e31021-e31029.

[86] M. Z. Aumeeruddy, M. F. Mahomoodally. (2019). Combating breast cancer using combination therapy with 3 phytochemicals: Piperine, sulforaphane, and thymoquinone. Cancer. 125 (10): e1600-e1611.

[87] M. Nikanjam, S. Liu, J. Yang, R. Kurzrock. (2017). Dosing three-drug combinations that include targeted anti-cancer agents: analysis of 37,763 patients. The oncologist. 22 (5): e576-e584.